A compact physical expression for the static drain current in heterojunction barrier CNTFETs

Manojkumar Annamalai and Michael Schröter

Chair for Electron Devices and Integrated Circuits (CEDIC), TU Dresden, 01062, Dresden, Germany

Abstract - A physics based compact expression for the static drain current in carbon nanotube field-effect transistors (CNTFETs) is presented, which takes into account the impact of heterojunction barriers at the source and drain end of the channel. The new formulation is based on a closed-form solution of the Landauer equation using a Gaussian-like surrogate function for its energy dependent integrand. The model also includes a smooth transition from thermionic emission based transport in the subthreshold region to tunneling dominated transport in the above-threshold regime. The formulation has been verified for both ballistic and scattering dominated carrier transport in the channel based on data obtained from device simulation of a unit cell structure and measurements of fabricated multi-tube high-frequency (HF) CNTFETs. Including the heterojunction barriers enables to capture the different curve shapes of the device characteristics and their differences in linearity compared to devices with ohmic con-

Keywords - Carbon nanotube field-effect transistor, compact modeling, drain current modeling.

I. INTRODUCTION

CNTFETs are promising candidates for future high-speed system-on-chip applications, including radio-frequency (RF) front-ends, possibly also integrated with digital CMOS electronics [1-3]. Analog HF CNTFETs fabricated at wafer-scale recently achieved cut-off frequencies around 100 GHz [4] which matches that of RF CMOS for the same channel length. For designing analog HF CNTFET circuits, a compact model is needed, which must accurately describe the drain current and tube charge over a wide bias range.

Existing compact drain current expressions that assume ohmic contacts (e.g., [5]) are not suitable for describing actual fabricated CNTFETs which exhibit a heterojunction barrier (HB) at the interface between the contact metal covered CNT and the oxide covered CNT in the channel [6,7]. As a consequence, the beyond-threshold drain current is determined by tunneling through that barrier. Compact drain current formulations using an energy independent tunneling transmission factor [8] are too inaccurate, while approaches that include the impact of HBs and are based on either Airy functions or even numerical integration of the Landauer equation [9-12] are computationally too expensive for circuit simulation and also contain model parameters that are difficult to determine by measurements. Given these challenges, this work presents a novel compact physics-based description for the drain current of HB CNTFETs that is based on a closed-form analytical solution of the Landauer equation. The single continuously differentiable formulation is valid for both Fermi- and Boltzmann statistics without the necessity of partitioning the energy (and hence the bias) region and includes the energy dependence of the transmission factor.

Device simulation is employed as reference for verifying the analytical solution for both ballistic and scattering dominated

transport. Moreover, the compact formulation is compared with measured data of a multi-tube HF CNTFET [12].

II. DEVICE SIMULATION

For the investigation pursued here, a 3D unit cell structure with a single n-type CNT shown in Fig. 1 was simulated. The unit cell may be part of a multi-tube CNTFET with the top gate electrode located symmetrically between source and drain contact. The simulation is facilitated by a computationally efficient simulation approach based on augmented drift-diffusion transport (aDD) including WKB boundary conditions for describing the tunneling current and coupled with a 3D Poisson solver [13].

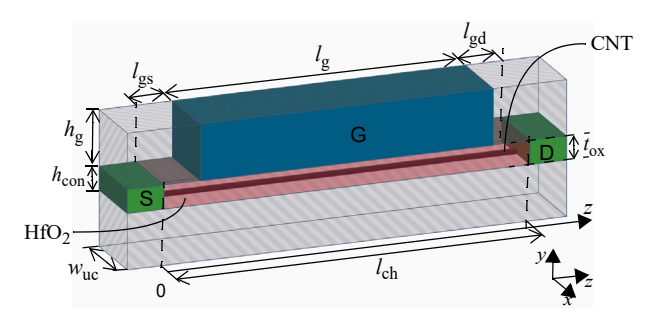


Fig. 1. 3D view of the simulated top-gate (tG) CNTFET unit cell within a multi-tube channel HF structure. $h_{\rm con}=6.3$ nm, $h_{\rm g}=15$ nm, $l_{\rm ch}=100$ nm, $t_{\rm ox}=6.3$ nm, $l_{\rm gs}=l_{\rm gd}=10$ nm.

The schematic band diagram, shown in Fig. 2, presents the different current components $(I_{\rm nS,th}, I_{\rm nS,tu})$ of the total source injected current as well as the influence of the internal gate and drain voltages $(V_{\rm G'S'}, V_{\rm D'S})$ on the conduction band edge $W_{\rm C}$. Also indicated is the possible multiple scattering of injected carriers between the barriers.

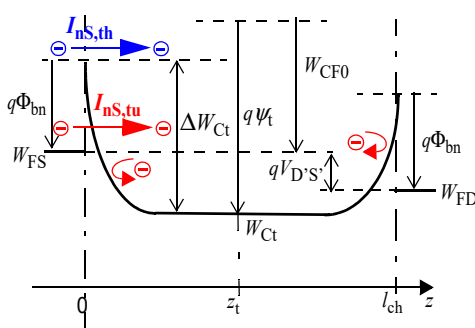


Fig. 2. Conduction band edge along the channel at low $V_{\rm D'S'}$ and high $V_{\rm G'S'}$ with $q\Phi_{\rm bn}$ as barrier height and definition of relevant variables; the tube surface potential $\psi_{\rm t}$ is defined against the equilibrium level of the conduction band $W_{\rm CF0}$ (= ${\rm q}V_{\rm CF0}$) relative to the source Fermi level $W_{\rm FS}$. $W_{\rm Ct}$ is the conduction band edge at location $z_{\rm t}$ in the middle of the channel under the gate. The drain Fermi level $W_{\rm FD}$ is shifted with respect to $W_{\rm FS}$ due to the applied $V_{\rm D'S'}$.

1

III. ANALYTICAL FORMULATION FOR THE STATIC DRAIN CURRENT

In static operation and in absence of impact ionization, recombination and direct source-drain tunneling, the drain current equals the transfer current. The latter results from the difference between the right (towards drain) and left (towards source) going carrier flux. The right going electron transfer current (index "n") injected by the source (index "S") can be calculated by the Landauer equation,

$$I_{\rm nS} \cong \frac{4q}{h} \int_{W_{\rm C}}^{\infty} T_{\rm n}(W) f_{\rm n}(W, W_{\rm FS}) dW, \qquad (1)$$

with $f_{\rm n}$ as the Fermi-function and $T_{\rm n}$ as the transmission factor for electrons flowing from source to drain. Generally, $T_{\rm n} = T_{\rm nS} T_{\rm n,ch} T_{\rm nD}$, where $T_{\rm nS}$ ($T_{\rm nD}$) represents the transmission through the source (drain) barrier region and $T_{\rm n,ch}$ the transmission along the remaining CNT channel region. For a HB FET, $T_{\rm nS}$ ($T_{\rm nD}$) dominates the carrier flow from S to D. Thus, solving Eq. (1) with $T_{\rm n} \approx T_{\rm nS}$ is expected to maintain the essential features of the source related transfer current. Then the same solution can be applied to the drain injected electron current.

A. Thermionic emission over the barrier

At low injection (subthreshold region) the conduction band edge underneath the gate at $z_{\rm t}$ exceeds the top of the barrier i.e., $W_{\rm FS}+q\Phi_{\rm bn}$, resulting in the thermionic emission of carriers over the barrier. The Landauer integral in Eq. (1) is solved analytically for the thermionic current $I_{\rm nS,th}$ by assuming an energy and bias independent transmission factor $\overline{T}_{\rm n.th}$,

$$I_{\text{nS,th}} = I_{\text{nth0}} \ln(1 + \exp(u_{\text{thS}})), \qquad (2)$$

with the model parameter $I_{\rm nth0} = G_{\rm q} V_{\rm T} \overline{T}_{\rm n,th}$ and $G_{\rm q} = 4q^2/h$ as the quantum conductance. The variable

$$u_{\text{thS}} = \frac{-\left(m_{\text{th}}V_{\text{T}}\ln\left(1 + \exp\left(-\frac{\eta_{\text{S}}}{m_{\text{th}}}\right)\right) + \Phi_{\text{bn}}\right)}{m_{\text{th}}V_{\text{T}}}$$
(3)

with $m_{\rm th}$ for adjusting the subthreshold slope and $\Phi_{\rm bn}$ as model parameters and $V_{\rm T}=k_{\rm B}T/q$ as the thermal voltage provide the desired smooth transition of the exponent argument in Eq. (2) from thermionic emission to tunneling dominated transport. Here, the normalized bias variable $\eta_{\rm S}=(V_{\rm G'S'}-V_{\rm fb})/V_{\rm T}$ is introduced, representing the difference between barrier height (flatband case with $V_{\rm fb}=V_{\rm CF0}-\Phi_{\rm bn}$) and equilibrium conduction band edge. $I_{\rm nS,th}$ increases with gate-source (GS) voltage until the flat band case, when the band edge $W_{\rm Ct}$ equals $W_{\rm FS}+q\Phi_{\rm bn}$. From thereon $I_{\rm nS,th}$ becomes bias independent and a function of just the barrier height.

Setting $\psi_t = V_{G^*S^*}$ is justified in subthreshold. Beyond that, an iterative solution is in principle required for ψ_t that causes additional computational burden though. This is avoided by using $V_{G^*S^*}$ instead. Therefore, all formulations presented here have been made a direct function of the internal terminal voltages $V_{G^*S^*}$ and $V_{D^*S^*}$, which are related to the voltages at the device terminals V_{GS} and V_{DS} respectively via series resistances.

B. Tunneling through the source hetero-barrier

With further increase in GS voltage, the conduction band edge at $z_{\rm t}$ drops below $W_{\rm FS}$ + $q\Phi_{\rm bn}$ and tunneling $(I_{\rm nS,tu})$

through the HB dominates the total source injected current. Also the transmission factor $T_{\rm nS}$ in the Landauer integral becomes strongly energy dependent. Since mostly the shape of the HB potential near the channel ends determines the transmission of the carriers, it is convenient to approximate the band edge with an exponential function given by

$$W_{C}(z) = W_{Ct} + \Delta W_{Ct} \exp(-z/l_b)$$
 (4)

with the characteristic length $l_{\rm b}$ as a model parameter and $\Delta W_{\rm Ct}$ defined in Fig. 2.

The approximation agrees well with the numerical simulation results as shown on the left side of Fig. 3. This allows to use the single energy point W_{Ct} in the middle of the channel at z_{t} that is coupled to the gate potential. With Eq. (4), the WKB approximation yields the analytical expression

$$T_{\rm nS}(W) = \exp\left(-4I_{\rm b}\sqrt{\frac{2m^*\Delta W_{\rm Ct}}{\hbar^2}}\left[\sqrt{1-w}-\sqrt{w}\,\arctan\left(\sqrt{\frac{1}{w}-1}\right)\right]\right) (5)$$

with the normalized energy $w = (W - W_{Ct})/\Delta W_{Ct}$. Eq. (5) agrees well with the result from device simulation.

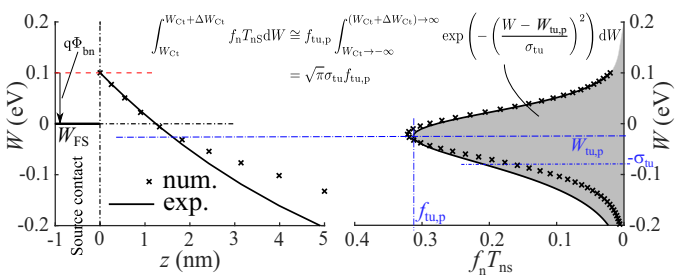


Fig. 3. Spatial dependence of conduction band edge near the source end of the channel (left) and example of the transmission distribution function versus energy (right).

The Landauer integrand, given by the transmission distribution function $f_{tu} = f_n T_{nS}$, is displayed on the right of Fig. 3. Realizing that the energy dependence of f_{tu} has the shape of a Gaussian, it can be approximated by

$$f_{tu}(\mathbf{W}) = f_{tu,p} \exp\left(-\left(\frac{\mathbf{W} - \mathbf{W}_{tu,p}}{\sigma_{tu}}\right)^{2}\right), \tag{6}$$

with its peak value $f_{tu,p}$ at $W_{tu,p}$ and σ_{tu} as its standard deviation. Eq. (6) allows to approximate the Landauer integral by

$$\int_{W_{Ct}}^{W_{Ct} + \Delta W_{Ct}} f_n T_{nS} dW \cong f_{tu,p} \int_{W_{Ct}}^{W_{Ct} + \Delta W_{Ct}} \exp\left(-\left(\frac{W - W_{tu,p}}{\sigma_{tu}}\right)^2\right) dW.$$
 (7)

Since the transmission distribution function and its Gaussian approximation decrease to negligible values towards the boundaries of the integration interval, the integration limits can be replaced by $\pm \infty$, yielding the simple closed-form solution for the source injected tunneling current

$$I_{\rm nS,tu} \cong \frac{4q}{h} \int_{(W_{\rm Ct} \to -\infty)}^{(W_{\rm Ct} + \Delta W_{\rm Ct}) \to \infty} f_{\rm n} T_{\rm nS} \ dW = \frac{4q}{h} \sqrt{\pi} \sigma_{\rm tu} f_{\rm tu,p} \ . \tag{8}$$

The integral, visualized by the shaded region on the right of Fig. 3, is close to the one obtained from device simulation.

Based on the observed behavior of $W_{tu,p}$ and σ_{tu} obtained from fitting a Gaussian profile to the transmission distribution function from numerical simulation shown in Fig. 4(a), their

GS bias dependence, especially the smooth transition from subthreshold to high-injection, is modeled by

$$\frac{\mathbf{W}_{\text{tu,p}}}{-\mathbf{q}} = V_{\text{tu,p}} = V_{\text{tup}} - \frac{V_{\text{tup}} + \Phi_{\text{bn}}}{\left[1 + \mathbf{b}_{\text{tup}} \ln(1 + \exp(\eta_{\text{S}}))\right]^{\mathbf{e}_{\text{tup}}}}$$
(9)

with the model parameters $V_{\rm tup}$, $b_{\rm tup}$ and $e_{\rm tup}$ and

$$\frac{\sigma_{\text{tu}}}{q} = V_{\text{\sigma tu}} f_{\text{\sigma,tu}}(\eta_{\text{S}}) = V_{\text{\sigma tu}} \left[m_{\text{\sigma tu}} \ln \left(1 + \exp \left(\frac{\eta_{\text{S}}}{m_{\text{\sigma tu}}} \right) \right) \right]^{e_{\text{\sigma tu}}}$$
(10)

with the model parameters V_{otu} , m_{otu} and e_{otu} , respectively. The bias dependent function $f_{\text{tu,p}}$, shown in Fig. 4(b), requires the evaluation of both the Fermi function and the transmission factor at the peak energy $W_{\text{tu,p}}$ of the transmission distribution. The DS voltage dependence seen in the observed behavior of $W_{\text{tu,p}}$, σ_{tu} and $f_{\text{tu,p}}$ is not included in the modeling of source related Gaussian variables but rather in the drain related variables and the discussion is given further below.

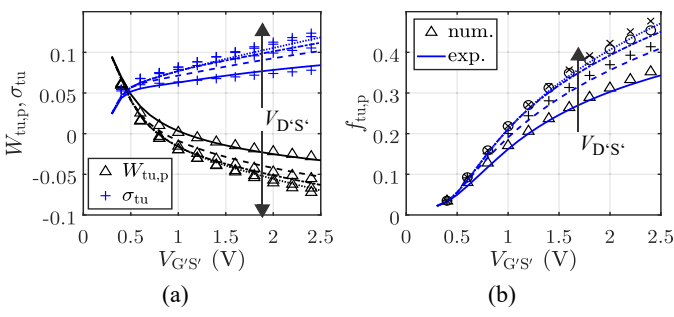


Fig. 4. Bias dependence of the variables determining the Gaussian approximation (6): (a) $W_{\rm tu,p}$ (Δ) and $\sigma_{\rm tu}$ (+) determined from $f_{\rm tu}$ with numerical $T_{\rm nS}$ (symbols) and using the analytical approximation (5) (lines). (b) $f_{\rm tu,p}$ calculated with numerical $T_{\rm nS}$ (symbols) and with the analytical approximation (5) (lines). The drain voltage dependence (for $V_{\rm D'S'}/V = 0.1, 0.25, 0.75, 2$) of $W_{\rm p,tu}$, $\sigma_{\rm tu}$, and $f_{\rm tu,p}$ is represented by different line styles. The data correspond to ballistic transport.

Carriers injected by tunneling experience scattering along the channel at higher drain-source (DS) voltages. This effect on the carrier velocity is taken into account by the computationally simple standard function for $T_{\rm n,ch}(V_{\rm D^{\circ}S^{\circ}})$ given by

$$T_{\text{n.ch}}(V_{\text{D'S'}}) \approx v_{\text{d}} / [1 + v_{\text{d}}^{e_{\text{DS.cr}}}]^{1/e_{\text{DS.cr}}}$$
 (11)

with the normalized variable $v_{\rm d} = |V_{\rm D'S'}|/V_{\rm DS,cr}$ while $V_{\rm DS,cr}$ and $e_{\rm DS,cr}$ are model parameters. Then, the compact formulation for the source injected tunneling current reads

$$I_{\text{nS,tu}} = I_{\text{ntu}0} f_{\sigma,\text{tu}} f_{\text{tu,p}} T_{\text{n,ch}}$$
 (12)

with the model parameter $I_{\rm ntu0} = G_{\rm q} \sqrt{\pi} V_{\rm \sigma tu}$ that absorbs all constant prefactors. Thus the total source injected current reads

$$I_{nS} = I_{nS.th} f_{th.tu} + I_{nS.tu} (1 - f_{th.tu}).$$
 (13)

where the function

$$f_{\text{th,tu}} = \left[1 + \exp\left(\frac{V_{\text{G'S'}} - m_{\text{thtu}} V_{\text{fb}}}{V_{\text{T}}}\right)\right]^{-1}$$
 (14)

provides a smooth transition between thermionic and tunneling regime. The model parameter m_{thtu} offers the flexibility for minor adjustment of flatband voltage.

The drain injected current component $I_{\rm nD}$ is calculated similarly. The drain injected thermionic current is computed from Eq. (2) by replacing $\eta_{\rm S}$ with $\eta_{\rm D}$ given by $\eta_{\rm D} = (V_{\rm G^*S^*} - V_{\rm D^*S^*} - V_{\rm fb})/V_{\rm T}$. For modeling drain injected tunneling current, the DS voltage dependence of the $\sigma_{\rm tu}$ is described by replacing $\eta_{\rm S}$ with $\eta_{\rm D}$ in Eq. (9) and the peak energy $W_{\rm tu,p}$ is modeled via

$$\frac{\mathbf{W}_{\text{tu,pD}}}{-\mathbf{q}} = V_{\text{tu,pD}} = \alpha_{\text{tup}} V_{\text{D'S'}} - \frac{\alpha_{\text{tup}} V_{\text{D'S'}} + \Phi_{\text{bn}}}{\left[1 + \mathbf{b}_{\text{tup}} \ln(1 + \exp(\eta_{\text{D}}))\right]^{\mathbf{e}_{\text{tup}}}}. (15)$$

Here the model parameter $V_{\rm tup}$ in Eq. (9) is replaced by $\alpha_{\rm tup}V_{\rm D^{\circ}S^{\circ}}$ with $\alpha_{\rm tup}$ as the model parameter. The static electron drain current $I_{\rm Tn}$ then reads

$$I_{\rm Tn} = I_{\rm nS} - I_{\rm nD} \,. \tag{16}$$

IV. RESULTS

Nonlinear optimization is used for determining the parameter values for a given set of $I_{\rm D}(V_{\rm G'S'},V_{\rm D'S'})$ data. While the parameters $\Phi_{\rm bn}$ and $V_{\rm CF0}$ are taken here directly from the device simulation, they have to be determined in practice from measured electrical data [14,15].

The resulting compact current expression yields good agreement with the device simulation results as shown in Fig. 5. The new formulation describes the smooth transition from the subthreshold to the high-injection region accurately, evident by the continuous and smooth transconductance in Fig. 5(b). As pointed out in [16], a hetero-barrier is required for obtaining high linearity (i.e. bias independent (flat) $g_{\rm m}$ curves). As shown in Fig. 5(b), the model is able to capture the respective curve shapes reasonably well, especially at high $V_{\rm D^4S^4}$ which is most important for linear amplifier design. Good agreement is also obtained for the output characteristics and output conductance (cf. Fig. 5(c), (d)), in particular in the bias region that is most revelant for RF circuit design. The observed deviations are attributed to backscattering from the heterobarrier at the drain end of the channel.

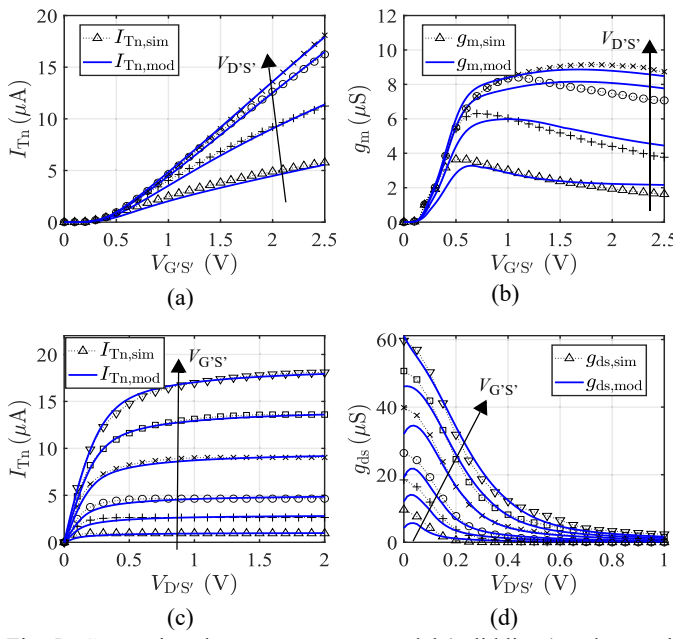


Fig. 5. Comparison between compact model (solid lines) and numerical simulation (symbols) of the structure in Fig. 1 with *ballistic* transport: (a), (b) transfer characteristic and transconductance for $V_{D'S'}$.

V = 0.1, 0.25, 0.75, 2; (c), (d) output characteristics and conductance for V_{G^*S} /V = 0.5, 0.75, 1, 1.5, 2, 2.5.

Drain current and conductances resulting from the device simulation of the tG structure with scattering dominated transport in the channel are shown in Fig. 6 for the same bias range as before. Carrier scattering along the channel significantly reduces the drain current for high $V_{\rm D^{\prime}S^{\prime}}$ and $V_{\rm G^{\prime}S^{\prime}}$ as the comparison with the results in Fig. 5 shows. Furthermore, carrier scattering causes a more peaky behavior of the transconductance and thus a less linear behavior of drain current. The new formulation is able to capture this behavior as well.

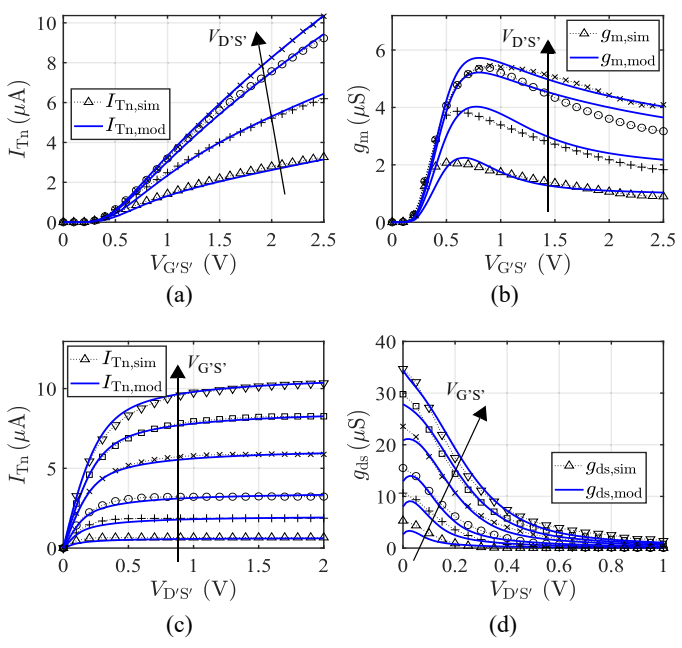


Fig. 6. Comparison between compact model (solid lines) and numerical simulation (symbols) of structure in Fig. 1 with *scattering* transport: (a), (b) transfer characteristic and transconductance for $V_{\rm D'S'}/V = 0.1, 0.25, 0.75, 2$; (c), (d) output characteristics and conductance for $V_{\rm G'S'}/V = 0.5, 0.75, 1, 1.5, 2, 2.5$.

The developed formulation has been integrated into the compact CNTFET model CCAM [17], which also includes all relevant parasitic elements of the complete fabricated transistor structure, such as series resistances from contacting the CNTs and the connection metal layer components as well as the corresponding parasitic capacitances. Excellent agreement of drain current and transconductance with measured data from the multi-tube HF CNTFET in [12] is observed in Fig. 7, confirming the suitability of the new current formulation also for fabricated devices.

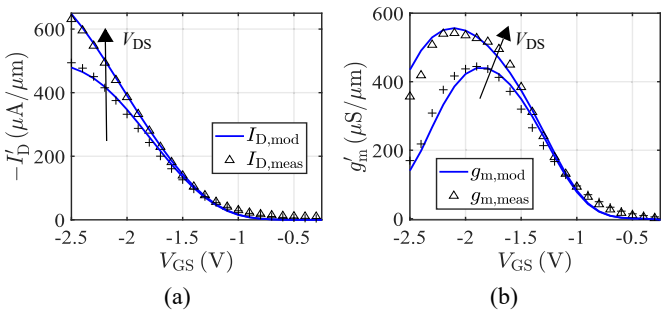


Fig. 7. Comparison between compact model (lines) and measurements (symbols) of the HF CNTFET in [12] for (a) drain current and

(b) transconductance as a function of the *terminal* voltages $V_{\rm GS}$ and $V_{\rm DS}/{\rm V}$ = -1, -1.5.

V. SUMMARY AND CONCLUSIONS

A physics-based compact formulation for the static drain current of CNTFETs has been derived that includes the impact of the contact hetero-barrier. The new expression is based on a closed-form solution of the Landauer equation using a surrogate function for its integrand. Comparisons to device simulation and experimental results show good agreement over a wide bias range. Although the formulation has been derived and presented for an electron current, with proper sign changes it can be applied also to the hole current component.

ACKNOWLEDGMENTS

The authors like to thank Dr. S. Mothes, formerly with CEDIC, for valuable discussions regarding the device simulator. This project has been financially supported in part by the German National Science Foundation (DFG SCHR695/23-2).

REFERENCES

- [1] Hartmann M, et al. CNTFET Technology for RF applications: review and future perspective. IEEE J. of Microwaves. 2021;1(1):275–87.
- [2] Cao Y, et al. Review of electronics based on single-walled carbon nanotubes. Top Curr. Chem. (Z). 2017;375(5):75.
- [3] Schröter M, et al. Carbon nanotube FET technology for radio-frequency electronics: State-of-the-art overview (invited). IEEE J. of the Electron Dev. Society. 2013;1(1):9–20.
- [4] Rutherglen C, et al. Wafer-scalable, aligned carbon nanotube transistors operating at frequencies of over 100 GHz. Nat. Electronics. 2019;2(11):530–9.
- [5] Marani R, Gelao G, Perri AG. Modelling of carbon nanotube field effect transistors oriented to SPICE software for A/D circuit design. Microelectronics J. 2013;44(1):33–8.
- [6] Fediai A, et al. Towards an optimal contact metal for CNTFETs. Nanoscale. 2016;8(19):10240–51.
- [7] Claus M, et al. COOS: a wave-function based Schrödinger–Poisson solver for ballistic nanotube transistors. J. Comput. Electron. 2014 Sep 1;13(3):689–700.
- [8] Zhang Y, Yang Y, Yang T, Zhang Y. A compact physical drain current model of multitube carbon canotube field effect transistor including diameter dispersion effects. IEEE Trans. on Electron Devices. 2021;68(12):6571–9.
- [9] Bejenari I, Schröter M, Claus M. Analytical drain current model of 1-D ballistic Schottky-barrier transistors. IEEE Trans. on Electron Devices. 2017;64(9):3904–11.
- [10] Vega RA. On the modeling and design of Schottky field-effect transistors. IEEE Trans. on Electron Devices. 2006;53(4):866–74.
- [11] Michetti P, Iannaccone G. Analytical model of one-dimensional carbon-based Schottky-barrier transistors. IEEE Trans. on Electron Devices. 2010;57(7):1616–25.
- [12] Cao Y, et al. Radio frequency transistors using aligned semiconducting carbon nanotubes with current-gain cutoff frequency and maximum oscillation frequency simultaneously greater than 70 GHz. ACS Nano. 2016;10(7):6782–90.
- [13] Mothes S, Schröter M. Three dimensional transport simulations and modeling of densely packed CNTFETs. IEEE Trans. on Nanotechnology. 2018;17(6):1282–7.
- [14] Pacheco-Sanchez A. Determination of key device parameters for shortand long-channel Schottky-type carbon nanotube field-effect transistors [PhD Thesis]. [Dresden]: Technische Universitat Dresden; 2019.
- [15] Ortiz-Conde A, et al. A review of recent MOSFET threshold voltage extraction methods. Microelectronics Reliability. 2002 Apr 1;42(4):583– 96.
- [16] Mothes S, Claus M, Schröter M. Toward linearity in Schottky barrier CNTFETs. IEEE Trans. on Nanotechnology. 2015 Mar;14(2):372–8.
- [17] Schröter M, et al. A semiphysical large-signal compact carbon nanotube FET model for analog RF applications. IEEE Trans. on Electron Devices. 2015;62(1):52–60.